Journal of
Synchrotron
Radiation

ISSN 0909-0495

Received 14 January 2008
Accepted 18 March 2008

High-resolution angular beam stability monitoring at a nanofocusing beamline

R. Tucoulou,* G. Martinez-Criado, P. Bleuet, I. Kieffer, P. Cloetens, S. Labouré, T. Martin, C. Guilloud and Jean Susini

ESRF, 38043 Grenoble CEDEX 09, France. E-mail: tucoulou@esrf.fr

Two semi-transparent imaging beam-position monitors developed at the ESRF have been installed at the micro-analysis beamline ID22 for monitoring the angular stability of the X-ray beam. This system allows low-frequency (10 Hz) angular beam stability measurements at a submicroradian range. It is demonstrated that the incoming macro-beam angular fluctuations are one of the major sources of focal spot instabilities downstream of the Kirkpatrick–Baez mirrors. It is also shown that scanning the energy by rotating the so-called fixed-exit monochromator induces some unexpected angular beam shifts that are, to a large extent, deterministic.

Keywords: beam-position monitoring; X-ray camera; nanoprobe.

1. Introduction

As nanofocusing optics are now becoming available for high-energy X-rays (see for example Kang *et al.*, 2006; Matsuyama *et al.*, 2006; Youn *et al.*, 2005; Hignette *et al.*, 2005; Schroer *et al.*, 2005; Jarre *et al.*, 2005; Yun *et al.*, 1999), many beamlines aiming at providing nanometre-scale lateral resolution are under construction. At the ESRF, the ID22NI nano-imaging end-station is one of three projects already approaching this high spatial resolution and preparing the general upgrade programme of the ESRF to be carried out during the forthcoming years. This nanoprobe is dedicated to the combination of three-dimensional imaging and micro-analysis fluorescence.

Combined with the expected increase of the synchrotron current (300 mA) and therefore of the higher heat load on the main optical elements, the operation of such a nanoprobe involves an accurate and real-time beam diagnostic to ensure a focal spot stability in agreement with the announced lateral resolution.

To our knowledge, most X-ray beam-position monitors are by definition only position-sensitive and do not provide any information about the stability of the angle of incidence which is by far the most critical parameter for nanofocusing optics: for example, in the case of reflective optics a variation of the incidence angles on the Kirkpatrick–Baez (KB) mirrors directly involves a focal spot drift and possibly a defocusing. With typical KB focal distances being of the order of 30 cm, an angular stability of the incident beam direction much below the μrad level is a prerequisite to preserving lateral resolution. In order to perform spectroscopic measurements at ID22NI, the focal spot position should be kept fixed even when the monochromator is rotated to select the energy over a few hundred eV. Although this monochromator is considered to be fixed-exit, small angular deviations of the outgoing beam cannot be avoided and should at least be evaluated and if possible compensated.

For several years, X-ray beam-position monitoring of submicrometre resolution based on an imaging system (YAG scintillator screen imaged by a CCD camera) has been developed at the ESRF and is currently used for beam diagnostics and KB mirrors focusing (Hignette *et al.*, 2007). Similar devices are also in use elsewhere for beam monitoring (Bunk *et al.*, 2005; Shenglan *et al.*, 2007). Thin and low-density scintillator and mirror have recently been developed to allow this system to be used as a semi-transparent real-time beam monitor. By using simultaneously two of these beam-position monitors (BPMs) separated by several metres, following the evolution of the beam angular direction is straightforward, and, by adding a third device in the focal plane of the KB mirrors, correlations between the angular stability of the incoming beam and the focal spot position can be established.

This paper focuses on the characterization of this 'beam vector finder' and on its use in investigating the position and angular stabilities of the X-ray beam at ID22 in two different modes. In the first part, a 'static' mode is investigated: the three BPMs measure the drifts of the beam position over long periods of several hours during which the current in the ring (and consequently the photon flux at the beamline) and the temperature in the hutch are the only parameters varying with time. In the second part, the aim is to study the position stability of the focal spot when a disturbance is introduced in the optics on purpose. We aimed at characterizing the focal spot stability during an energy scan.

2. Beamline layout

The ID22 beamline is described in detail by Somogyi *et al.* (2005). The main characteristics are summarized hereafter. The ID22 high-β straight section is equipped with two undulators covering an energy range from 6 to 70 keV. The beamline is equipped with a flat horizontally reflecting mirror (Si, Pd, Pt coatings) and a double-crystal [Si(111) or (311)] fixed-exit Kohzu monochromator (DCM). High-power slits can be used to define a secondary source at 27 m from the main one. Two experimental hutches (EH1–2) are installed at 41 and 63 m from the source. Both use dynamically bent KB mirrors to focus the beam. They mainly differ by the lateral resolution which goes from the micrometre scale for EH1 down to 80–120 nm for EH2. In EH1 the focus is obtained by a demagnified image of the primary source while in EH2 a horizontal secondary source is created by closing the high-power slits down to 40 µm. The distances between the source and the main optical components are given in Fig. 1. In EH2 (nanoprobe set-up) the focal length of the vertically (horizontally) focusing mirror is 280 mm (95 mm).

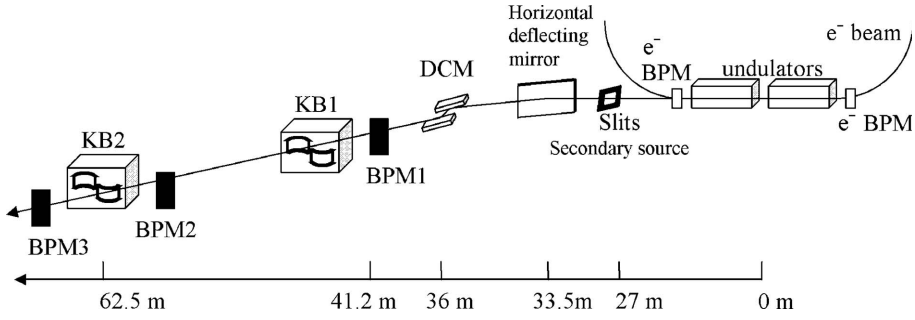

Figure 1
Beamline layout (not to scale).

3. Description of the imaging system

This imaging BPM (see Fig. 2) is based on a commercially available 100 µm-thick Al_2O_3:Ti scintillator screen, coupled to a polished 200 µm-thick beryllium foil of 0.1 µm roughness used as a mirror oriented at 45°, both of them being semi-transparent to X-rays (30% total absorption at 16 keV). An opto-mechanical device is used to hold the free-standing sapphire screen, the mirror, an achromatic doublet and a CCD camera. The two achromatic lenses of 50 mm focal length provide a one-to-one magnification. A digital Sony XC710 camera is used, offering the convenience of the IEEE-1394 interface, *i.e.* a standard communication protocol, high-speed data transfer and power supply in a single cable. Compact, light and inexpensive, this camera can reach up to 30 frames s^{-1} in full frame with no binning (1024 × 768 pixels). An external trigger mode is used to read several cameras synchronously. The pixel size is 4.65 µm and the field of view is 4.8 × 3.6 mm. The exposure time can be set up from 10 µs to 17 s. The camera is interfaced with a Linux device server *via* IEEE1394a including the major BPM calculations [beam position, full width at half-maximum (FWHM) *etc.*].

For the third BPM placed in the focal plane of the KB mirrors (see Fig. 1), the optical head is slightly different from the two others since there is no need for transparency. A 25 µm-thick YAG crystal grown by epitaxy is used as a scintillator and the mirror is made of polished glass coated with Al. The pixel size is 3 µm in this case.

The beam position is determined by integrating the image over each direction and by using a Fourier-transform centroid algorithm based on the maximization of the intercorrelation function. BPM1 and BPM2 image a macroscopic beam of several hundred micrometres, therefore the integration time must be set to a much higher value than for BPM3 which receives more or less the same photon flux but confined in a microscopic beam illuminating a very few pixels. This implies the use of external triggering to start the image acquisition on each BPM synchronously but to set separately by software the acquisition time of each BPM. On average, integration times are of the order of 0.02 s, 0.1 s and 0.001 s for BPM1, BPM2 and BPM3, respectively, for a 200 mA current in the ring. The standard deviation of the centre of mass during a time scan can be considered as a good indicator of the overall level of noise (including camera noise, vibrations *etc.*) in the frequency range limited by the exposure time. In the case of long-term-stability measurements, it can be helpful to refine the centre of mass determination by averaging over a series of successive short exposure times. This allows the high-frequency noise to be decreased without reaching CCD saturation.

One of the problems encountered with this kind of X-ray camera is that the determination of the beam position depends to some extent on the incoming intensity. This specifically happens when too many pixels are saturated or, on the other hand, when the intensity is too low with respect to the electronic noise. Comparing the focal spot position at two different energies separated by several keV is not straightforward since the intensity can vary significantly on the CCD and the integration time must be changed (adding attenuators

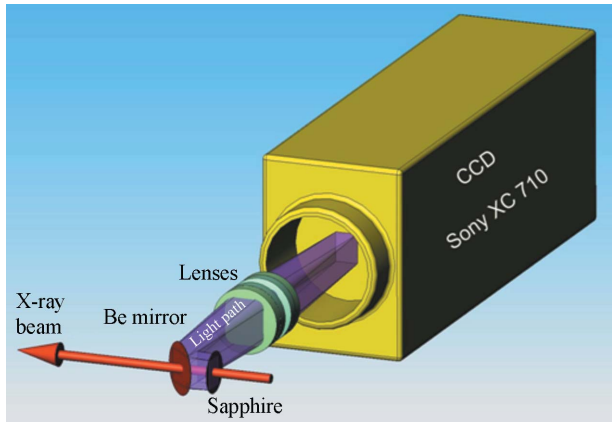

Figure 2
Optical scheme of the BPM.

is possible but involves a variation of heat load on the optics and may introduce intensity inhomogeneity which might influence the calculation of the beam position).

In order to reach sufficient sensitivity in the beam angle calculation, BPM1 and BPM2 are separated by a long distance of 21 m: BPM1 is situated in EH1 at 41 m from the source with BPM2 just before the KB mirrors in EH2. It should be noted that BPM2, the KB mirrors and BPM3 are mounted on the same rigid granite table in order to decrease relative drifts as much as possible.

The intrinsic sensitivity (defined as the smallest detectable beam displacement) of each BPM imaging the macroscopic beam (0.7 mm × 0.7 mm slits aperture upstream of BPM1) has been evaluated by moving the cameras by small steps in both directions. BPM1 and BPM2 give similar results: the minimum displacement they can detect is approximately 1 µm. This is the smallest step inducing a detectable change in the centre-of-mass average position (which is the result of the measurement noise of the system added to the overall vibration level of the beamline). Since the distance between BPM1 and BPM2 is 21 m, the angular sensitivity is in the range of 0.05 µrad. As mentioned in the *Introduction*, and in the context of nanometre resolution, the range of angular instabilities to deal with is below the microradian.

The sensitivity of BPM3 placed in the focal plane has been measured elsewhere (Hignette *et al.*, 2007) and estimated to approximately 3 nm. This much higher sensitivity in the focal plane is directly related to the smaller beam size. Typical standard deviations of the focal spot position at ID22NI (measured at 200 Hz and at a short time scale) are of the order of 15 nm (r.m.s.) including of course vibrations.

In the case of a submicrometre spot size, it is essential for the precision of the measurement to define a region of interest around the spot and to restrict the calculation of the beam position to this region (otherwise the contribution of the noise may change the result). To demonstrate the level of accuracy of this X-ray camera-based focal spot monitoring, Fig. 3 compares the results obtained using a BPM and using the standard knife-edge scan technique when the energy is moved from 13.1 to 13.7 keV for a focal spot size of 2 µm (the experiment was performed in EH1). As more specifically studied in the second part of the paper, this energy change induces some focal spot drifts which are measured by the two different techniques. The maximum discrepancy is 0.4 µm even though measurements could not be made at the same time: two successive energy scans separated by 15 min were performed, one for each method. The main advantage of the imaging system method is obviously the very short time required for the full focal spot position characterization (both directions are measured at the same time and in a single shot instead of two knife-edge scans for each energy step).

4. Preliminary tests

To make sure that the BPMs are correctly working, a basic test consists of inducing a known angular shift and to compare it with the one calculated from the BPM measurements.

For example, one can make a rocking curve of the second crystal of the monochromator and follow the vertical beam position for each angular step. Fig. 4 shows the rocking curve at 18 keV and the linear response of both BPMs. Within the angular FWHM, BPM1 (BPM2) measures a vertical displacement ΔY_1 (ΔY_2) of 190 µm (978 µm) which is consistent with the distances between the monochromator and both BPMs (5.2 and 26.5 m) and gives an angle of 37 µrad. The crystal rotation (piezo driver) is not angularly calibrated; nevertheless, this value can be compared with the double of the theoretical rocking-curve FWHM of a Si(111) crystal at 18 keV, *i.e.* 20.4 µrad. In the case of a pure rotational perturbation, these two BPMs allow in principle not only the determination of the amplitude of the angular variation but also of the position of the centre of rotation along the beam axis and therefore identification of the optical element responsible for the instability.

Rotating the second crystal of the monochromator is equivalent to moving 'virtually' the X-ray source by an amount which can be calculated from the angle given by the

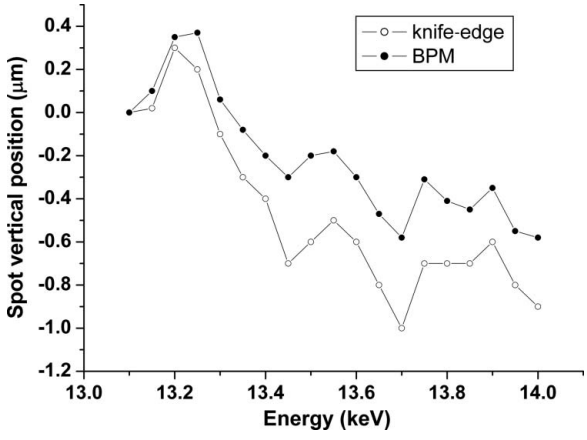

Figure 3
Focal spot position determined by two different techniques: knife-edge scan and X-ray BPM.

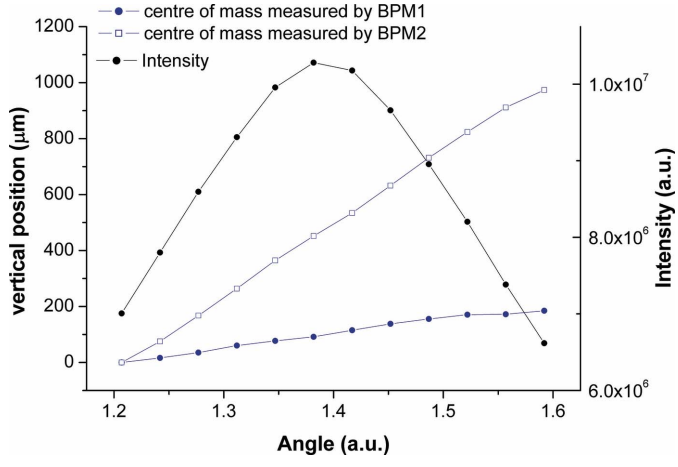

Figure 4
Responses of BPM1 and BPM2 during a rocking-curve scan of the second monochromator crystal at 18 keV.

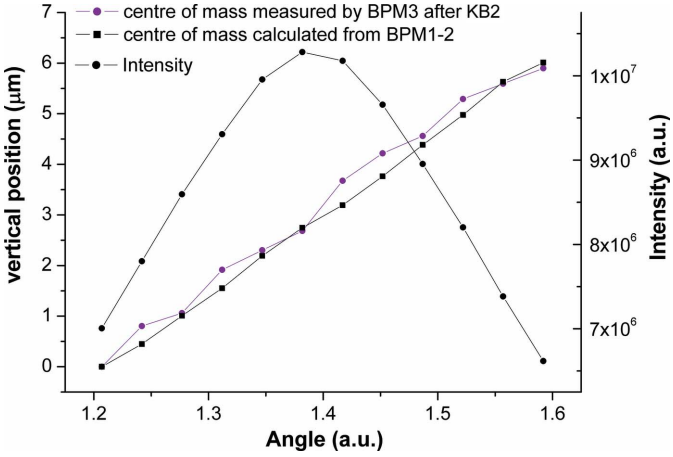

Figure 5
Focal spot drift measured with BPM3 during a rocking-curve scan compared with the drift calculated from BPM1 and BPM2 measurements.

BPMs and the monochromator–source distance. The variation of the incidence angle on the vertically focusing mirror is directly related to the source displacement and involves a vertical shift of the focal spot,

$$\partial \mathrm{FS_V} = f_\mathrm{V} \frac{(\Delta Y_2 - \Delta Y_1)}{(Z_2 - Z_1)} \frac{Z_\mathrm{mono}}{Z_\mathrm{KB}}, \qquad (1)$$

where Z_1, Z_2, Z_mono and Z_KB are the distances to BPM1, BPM2, the monochromator and the KB mirror from the source (or the secondary one if any), and f_V is the focal distance of the KB vertically focusing mirror.

Fig. 5 compares the real vertical position of the focal spot measured by BPM3 with the expected one calculated from BPM1 and BPM2, the monochromator–source and KB–source distances and the focal distance. The good agreement between the two curves shows that, in case of an angular drift of the X-ray beam owing to any optical element, the induced spot movement after the KB can be predicted from the vector finder measurements.

5. Low-frequency beam instabilities

To analyze low-frequency (10 Hz) beam instabilities, some time scans running over long periods of several hours have been acquired. The filling mode of the electron bunches in the ring was the so-called uniform mode (maximum current of 200 mA) with a refill every 12 h.

The energy was set to 18 keV and the exposure times for BPM1, BPM2 and BPM3 were set to 0.05, 0.2 and 0.005 s, respectively. Fig. 6 shows the vertical and horizontal positions of the centre of mass over 14 h measured by BPM1 and BPM2. The beam moved vertically by 75 μm in BPM1 and 350 μm in BPM2 giving a total angular excursion of approximately 14 μrad. The beam is more stable horizontally with only a 3 μrad drift and a strong variation of 2 μrad occurring during the refill. It should be noted that these rather large fluctuations are partially due to a failure of the global feedback correction of the electron orbit in the ring during the full measurement time. Simultaneously to the position monitoring of the X-ray

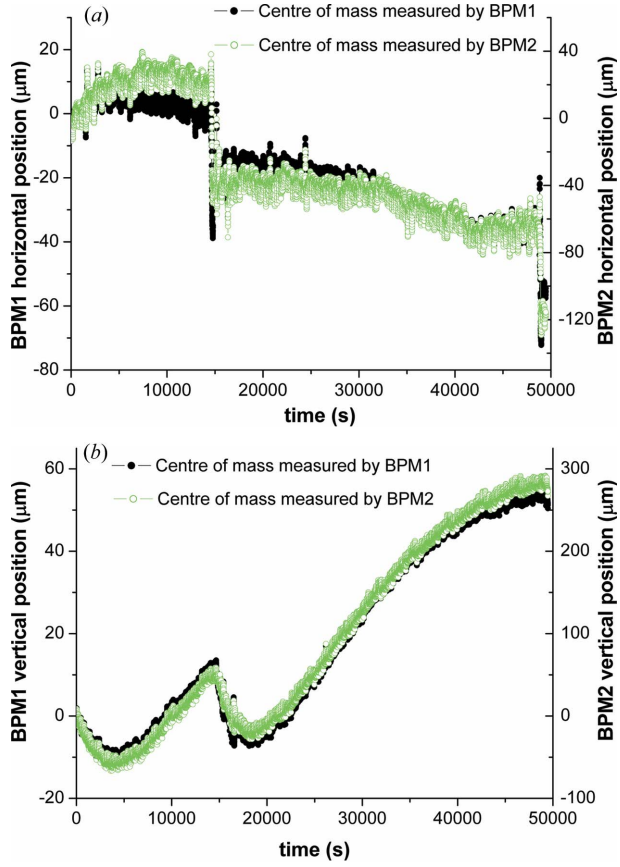

Figure 6
Long-term monochromatic beam-position monitoring with BPM1 and BPM2. (*a*) Horizontal, (*b*) vertical.

beam, the electron beam is also locally monitored with two BPMs located on each side of the ID22 straight section and separated by 5 m. It is interesting to compare the angular stability of both beams simultaneously. Fig. 7 clearly shows that the horizontal beam angles are correlated whereas this is not the case vertically. This shows that one optical element (most likely the monochromator) introduces some vertical fluctuations with much stronger amplitude than the one generated by the electron beam itself.

Fig. 8 shows the vertical focal spot position after the KB mirror (measured by BPM3) and the expected one calculated from the virtual source displacement associated with the angular drift measured from BPM1/2 and from the vertically focusing mirror focal distance (f_V = 0.28 m). Contrarily to the previous case where a disturbance was introduced by a crystal rotation at a known position, the sources of instabilities are unknown and multiple. Any optical element (including the X-ray source itself) may present some long-term drifts inducing some fluctuations of the virtual source position (and therefore of the incidence angle by which the KB mirrors 'see' the source). Equation (1) can be generalized to determine the induced focal spot vertical drift $\delta \mathrm{FS_V}$ from the variations of BPM1/2 (ΔY_1 and ΔY_2),

$$\partial \mathrm{FS_V} = f_\mathrm{V} \frac{(Z_1 \Delta Y_2 - Z_2 \Delta Y_1)}{(Z_2 - Z_1) Z_\mathrm{KB}}. \qquad (2)$$

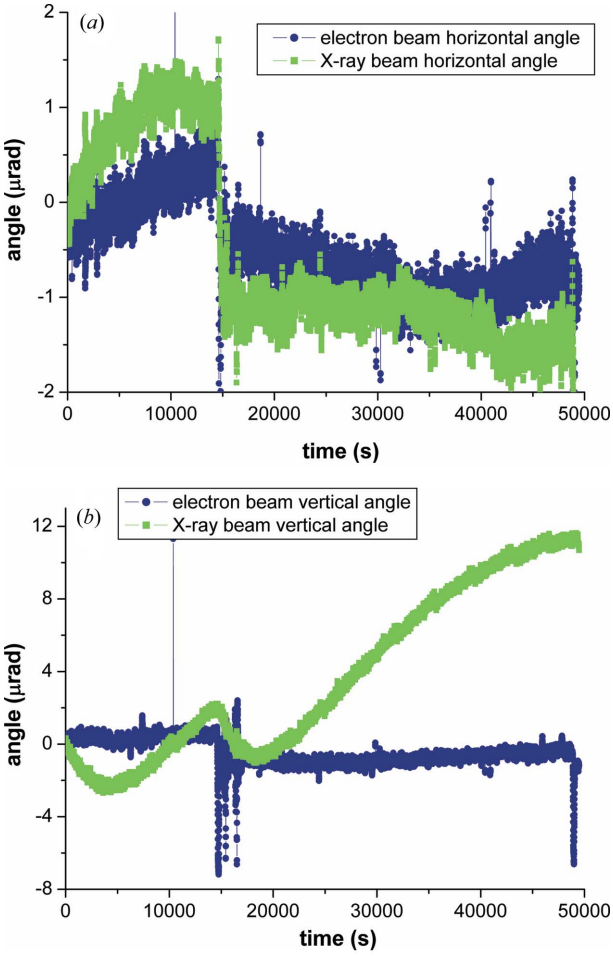

Figure 7
Long-term angular monitoring of electron and monochromatic X-ray beams. (*a*) Horizontal, (*b*) vertical.

It should be noted that if the source itself moves in emission angle (and not in position), $Z_1\Delta Y_2 - Z_2\Delta Y_1 = 0$, it should therefore have no effect on the focal spot position.

BPM3 gives a total vertical drift of approximately 4 μm over the full time scan which is by far much less than for the incoming beam on the KB mirror (350 μm measured by BPM2). It can be seen that there is an obvious correlation with the calculated drifts according to equation (2); nevertheless, the two curves do not superimpose meaning that the long-term position of the focal spot does not exclusively depend on the stability of the incoming incidence angle.

Owing to various thermal expansion coefficients of the different components of the mirrors' holder, their positions are sensitive to temperature fluctuations inside the hutch. However, it has been shown by Mokso (2006) that the radii of curvature of both mirrors remain stable in a first approximation by a correct choice of materials and that it is mostly the angles that change. Moreover, the BPM stage can show a differential thermal drift with respect to the optics holder. The EH2 experimental hutch is therefore thermally accurately regulated at $\pm 0.1^\circ$; nevertheless, the KB bender/mirror temperature follows, with a little delay, the evolution of the hutch temperature. The temperature of one KB mirror was

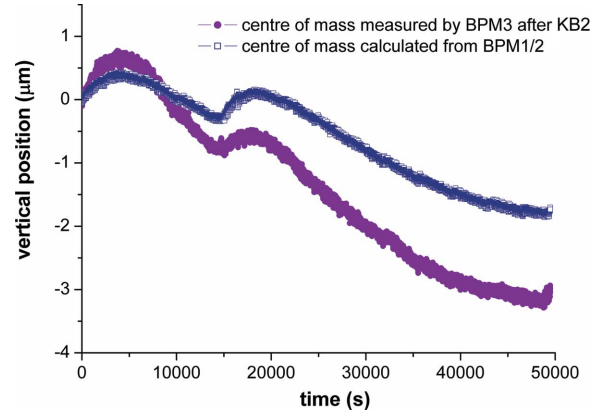

Figure 8
Comparison of measured (BPM3) and calculated (BPM1 and BPM2) focal spot position.

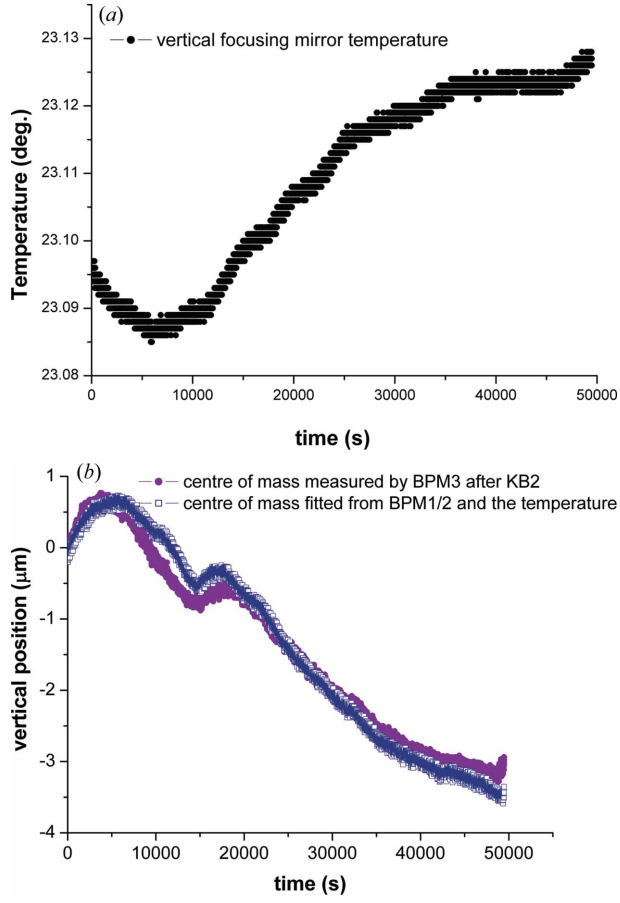

Figure 9
(*a*) Long-term temperature fluctuations of the vertically focusing mirror. (*b*) Linear fit of the vertical focal spot position with both the temperature and the incidence angle (from BPM1 and BPM2).

thus also measured during the time scan and is presented in Fig. 9(*a*). A maximum ΔT of 0.05° is measured over the full time scan. Fig. 9(*b*) shows that the vertical focal spot position can be very nicely fitted by a linear combination of the effects of the variations of the virtual source position and of the temperature ($\delta \mathrm{FS_V} + k\Delta T$). The discrepancy observed in Fig. 8 almost completely disappears as soon as the thermal drifts are

taken into account confirming that very accurate temperature regulation of the experimental hutch is essential for sub-micrometre lateral resolution preservation with time.

6. Focal spot stability during an energy scan

Keeping the focal spot fixed during an energy scan is a major issue for preserving the 'static' lateral resolution and is becoming more and more difficult to achieve with nanobeams. The aim of this study is to investigate the influence of the so-called fixed-exit ID22 monochromator on the focal spot stability and to see if the X-ray BPMs could be used to measure (and later compensate) eventual deterministic errors.

As a preliminary test, BPM3 is used to check the level of repeatability of the focal spot shifts between two identical energy scans. With the KB mirrors of the nanobeam end-station being coated with multilayers, the energy range is fixed by the multilayer bandwidth (from 17.6 to 18.8 keV in our case for the chosen incident angle). To further improve the precision of the beam monitoring and partially avoid some parasitic noise, the beam position is measured 30 times successively and averaged for each energy step (same exposure time as in the previous parts). Fig. 10 shows the beam monitoring results for two identical energy scans over 1 keV with 2 eV steps and measured at intervals of a few minutes. For each energy step the monochromator rotates the two crystals and adjusts the

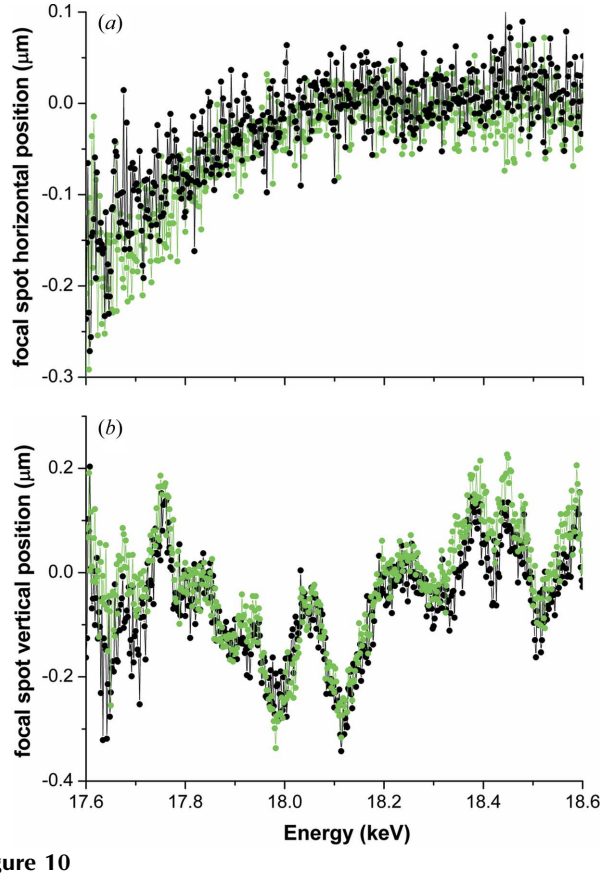

Figure 10
Focal spot position (measured by BPM3) *versus* energy for two successive scans. (*a*) Horizontal, (*b*) vertical.

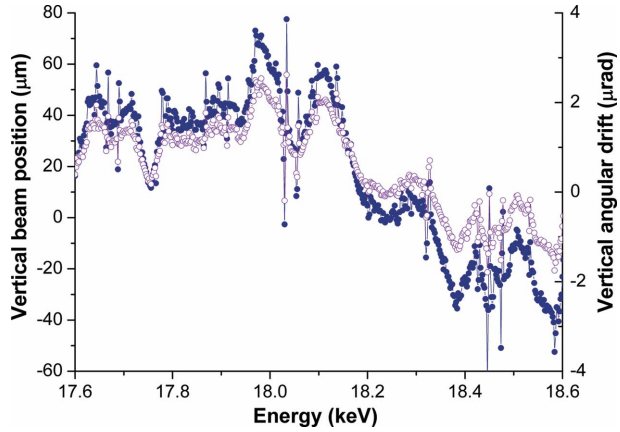

Figure 11
Direct beam position (measured by BPM2, full circles) and angle (from BPM1 and BPM2, open circles) during an energy scan.

distance between them for keeping the beam at the same position. BPM3 measures vertical (horizontal) focal spot movements of 0.5 μm (0.35 μm) over the full scanned energy range. It confirms that intrinsically there is no chance of keeping the spatial resolution down to 100 nm when the energy is scanned at ID22 (this monochromator was originally designed for micrometre-scale spectroscopic measurements). However, it seems that the focal spot drifts are, to a large extent, deterministic. Indeed, in the worst case the focal spot vertical (horizontal) position difference between the two scans is approximately 200 nm (250 nm). Even though this value is still too high to ensure a perfect focal spot stability, these curves clearly demonstrate that one can rely on a focus position monitoring performed just before an EXAFS acquisition to evaluate the most significant focal spot drifts *versus* the energy and to compensate them by moving the sample accordingly.

Using BPM1 and BPM2 the angular and spatial deviations of the incoming beam induced by the rotation of the monochromator can be calculated as presented in Fig. 11. The beam moves vertically by 120 μm just in front of the KB mirror while the total angular deviation of the beam direction reaches 4 μrad.

As noted previously, equation (1) can be used to predict the displacements of the focal spot from BPM1 and BPM2. Fig. 12 shows the good agreement between the calculated and measured (BPM3) vertical focal spot drifts. The two curves are strongly correlated, showing that most of the focal spot movements are induced by the angular fluctuations of the incoming beam direction. Nevertheless, the calculated and measured curves do not exactly superimpose, meaning that one cannot rely only on BPM1/2 to predict perfectly the spot drifts. A better accuracy is obtained by measuring the focal spot fluctuations with BPM3 before the real experiment on a sample rather than with BPM1 and BPM2 used as in-line real-time monitors. The first option also has the advantage of avoiding the presence of diffracting objects along the incoming beam path which may introduce glitches in the I_0 flux.

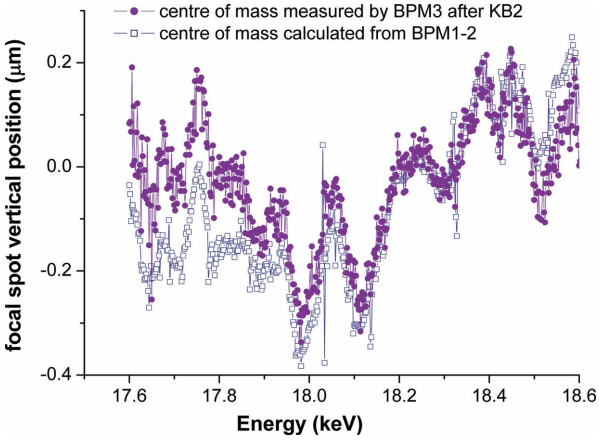

Figure 12
Comparison between measured (BPM3) and calculated (from incidence angle) focal spot position during an energy scan.

7. Conclusion

The presented vector finder method is a very promising tool for monitoring the angular stability of X-ray beams. Provided it can remain in the beam, it can be used as a simple real-time beam-position monitor but it can also be very helpful in the investigation of instabilities and for the understanding of their consequences on the focused beam position. At ID22 it has been shown that the fluctuations of the monochromatic focal spot position can be fully correlated to a combination of thermal mechanical drifts and of instabilities of the incidence angles. The vector finder method can be used to predict and compensate for focal spot movements, for example when performing an energy scan. It can also be used to decouple translation from rotation mechanical instabilities.

It has been studied up to now as a BPM of the overall beam stability, but, placed upstream and downstream of a given optical element, it might provide some interesting information on the intrinsic behavior and on the contribution to the global beamline stability of this optical element.

The first generation of sapphire scintillators is 100 μm thick which is still quite large regarding photon absorption. The next generation should be only 20 μm thick. The Be mirror and the sapphire scintillator should be more carefully polished to avoid downstream front wave distortion and possibly a worsening of lateral resolution after focusing.

References

Bunk, O., Pfeiffer, F., Stampanoni, M., Patterson, B. D., Schulze-Briese, C. & David, C. (2005). *J. Synchrotron Rad.* **12**, 795–799.
Hignette, O., Cloetens, P., Morawe, C., Borel, C., Ludwig, W. & Bernard, P. (2007). *AIP Conf. Proc.* **879**, 792–795.
Hignette, O., Cloetens, P., Rostaing, G., Bernard, P. & Morawe, C. (2005). *Rev. Sci. Instrum.* **76**, 063709.
Jarre, A., Fuhse, C., Ollinger, C., Seeger, J., Tucoulou, R. & Salditt, T. (2005). *Phys. Rev. Lett.* **94**, 074801.
Kang, H. C., Maser, J., Stephenson, G. B., Liu, C., Conley, R., Macrander, A. T. & Vogt, S. (2006). *Phys. Rev. Lett.* **96**, 127401.
Matsuyama, S., Mimura, H., Yumoto, H., Sano, Y., Yamamura, K., Yabashi, M., Nishino, Y., Tamasaku, K., Ishikawa, T. & Yamauchi, K. (2006). *Rev. Sci. Instrum.* **77**, 103102.
Mokso, R. (2006). PhD thesis, Université Joseph Fourier, Grenoble, France.
Schroer, C. G., Kurapova, O., Patommel, J., Boye, P., Feldkamp, J., Lengeler, B., Burghammer, M., Riekel, C., Vincze, L., Van der Hart, A. & Küchler, T. (2005). *Appl. Phys. Lett.* **87**, 124103.
Shenglan, X., Fischetti, R. F., Benn, R. & Corcoran, S. (2007). *AIP Conf. Proc.* **879**, 1403–1406.
Somogyi, A., Tucoulou, R., Martinez-Criado, G., Homs, A., Cauzid, J., Bleuet, P., Bohic, S. & Simionovici, A. (2005). *J. Synchrotron Rad.* **12**, 208–215.
Youn, H. S., Baik, S. Y. & Chang, C. (2005). *Rev. Sci. Instrum.* **76**, 023702.
Yun, W., Lai, B., Cai, Z., Maser, J., Legnini, D., Gluskin, E., Chen, Z., Krasnoperova, A. A., Vladimirsky, Y., Cerrina, R., Di Fabrizio, E. & Gentili, M. (1999). *Rev. Sci. Instrum.* **70**, 2238.